Expanded View Figures

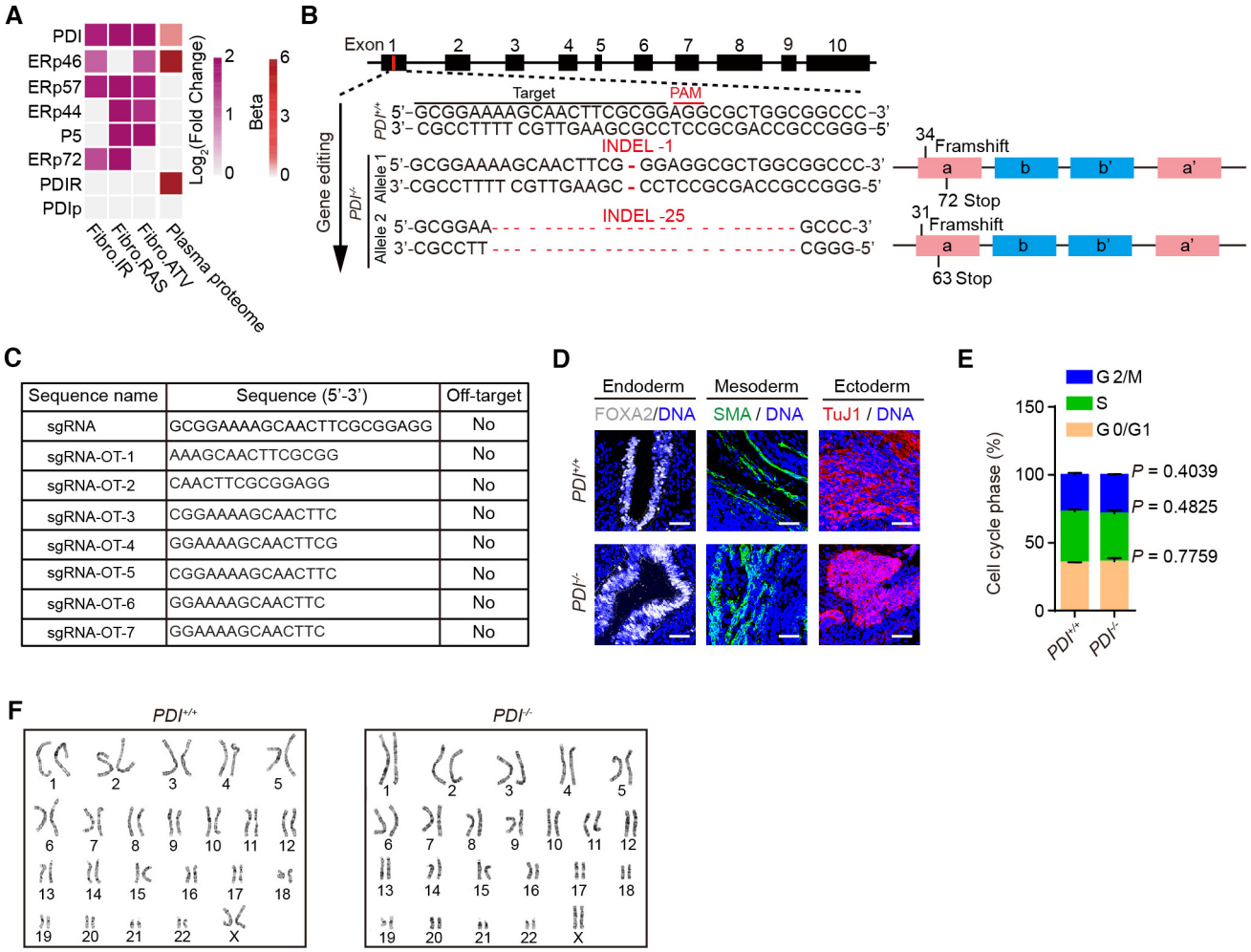

Sequence name	Sequence (5'-3')	Off-target
sgRNA	GCGGAAAAGCAACTTCGCGGAGG	No
sgRNA-OT-1	AAAGCAACTTCGCGG	No
sgRNA-OT-2	CAACTTCGCGGAGG	No
sgRNA-OT-3	CGGAAAAGCAACTTC	No
sgRNA-OT-4	GGAAAAGCAACTTCG	No
sgRNA-OT-5	CGGAAAAGCAACTTC	No
sgRNA-OT-6	GGAAAAGCAACTTC	No
sgRNA-OT-7	GGAAAAGCAACTTC	No

Figure EV1. Generation and characterization of *PDI*$^{-/-}$ hESCs.

A Conjoint analysis showing the secretion levels of PDI and its family members in SASPs (www.saspatlas.com) from multiple senescence inducers and in plasma proteome from 3,087 healthy individuals (Basisty *et al*, 2020; Ritchie *et al*, 2021). ATV, atazanavir treatment; RAS, inducible RAS overexpression; IR, X-irradiation. The color keys that change from white to dark purple represent the fold change of gene and protein, change from white to red represent the change in protein levels per unit increase in the covariate in plasma proteomic.

B Illustration of PDI gene editing (exon 1) via CRISPR/Cas9-mediated non-homologous end joining (NHEJ) in H9 hESCs. The sequences of the mutated alleles in *PDI*$^{-/-}$ hESCs depicting the deletions were shown. The INDELs caused a frameshift and leaded to an early termination.

C Analysis of the off-target of *PDI*$^{-/-}$ hESCs using genomic DNA PCR and sequencing. Predicted off-target sites against sgRNA and sgRNA sequences were presented in the table.

D Immunostaining of the FOXA2 (endoderm), SMA (mesoderm) and TuJ1 (ectoderm) in teratomas derived from *PDI*$^{+/+}$ and *PDI*$^{-/-}$ hESCs. Scale bar, 50 μm.

E Cell cycle analysis of *PDI*$^{+/+}$ and *PDI*$^{-/-}$ hESCs, Data are shown as mean ± SEM, $n = 3$ biological repeats, two-tailed Student's *t*-test.

F Karyotyping analysis of *PDI*$^{+/+}$ and *PDI*$^{-/-}$ hESCs.

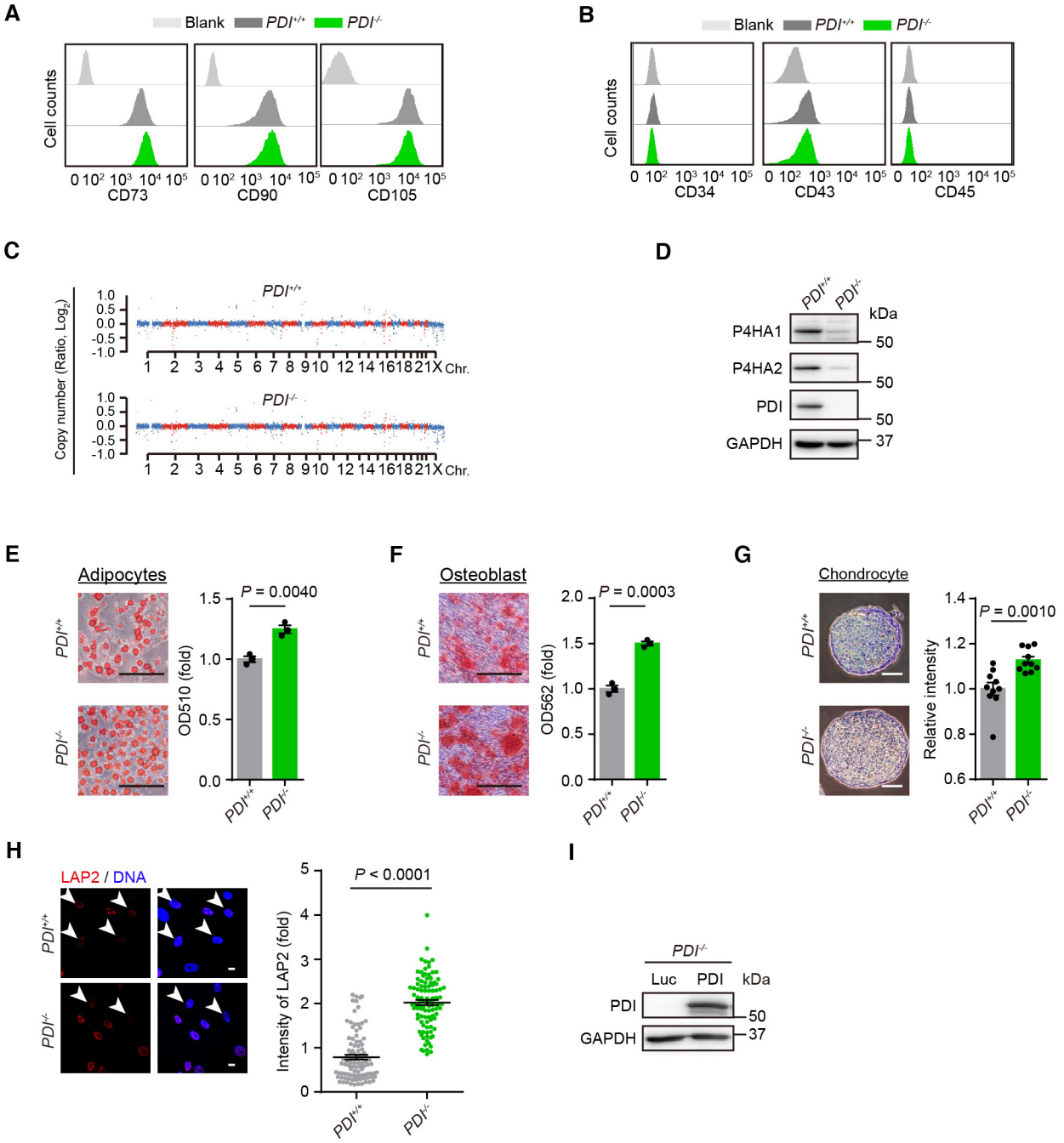

Figure EV2.

Figure EV2. Generation and characterization *PDI*$^{+/+}$ and *PDI*$^{-/-}$ hMSCs.

A FACS analysis for the *PDI*$^{+/+}$ and *PDI*$^{-/-}$ hMSC positive markers including CD73, CD90 and CD105.
B FACS analysis for the *PDI*$^{+/+}$ and *PDI*$^{-/-}$ hMSC negative markers including CD34, CD43 and CD45.
C Genome wide analysis of CNV of *PDI*$^{+/+}$ and *PDI*$^{-/-}$ hMSCs.
D Western blotting of the P4HA1 and P4HA2 protein in *PDI*$^{+/+}$ and *PDI*$^{-/-}$ hMSC. GAPDH was used as the loading control.
E Oil Red-O staining was used to characterize adipogenesis of *PDI*$^{+/+}$ and *PDI*$^{-/-}$ hMSC. The absorbance at 510 nm was measured. Scale bar, 200 μm. $n = 3$ biological repeats.
F Alizarin Red S staining was used to characterize osteogenesis of the *PDI*$^{+/+}$ and *PDI*$^{-/-}$ hMSC. The absorbance at 562 nm was measured. Scale bar, 200 μm. $n = 3$ biological repeats.
G Toluidine blue staining was used to characterize chondrogenesis of *PDI*$^{+/+}$ and *PDI*$^{-/-}$ hMSC. Scale bar, 100 μm. The intensity of the chondrocyte staining was measured. $n = 10$ biological repeats.
H Left, Immunostaining of the LAP2 expression in *PDI*$^{+/+}$ and *PDI*$^{-/-}$ hMSCs at P8. White arrowheads indicate cells with decreased LAP2 expression. Scale bar, 20 μm. Right, statistical analysis of the fluorescence of LAP2. $n = 100$ cells.
I Western blotting of the PDI expression in *PDI*$^{-/-}$ hMSCs transduced with Luc or PDI. GAPDH was used as the loading control.

Data information: In (E–H), data are presented as mean ± SEM, two-tailed Student's *t*-test.

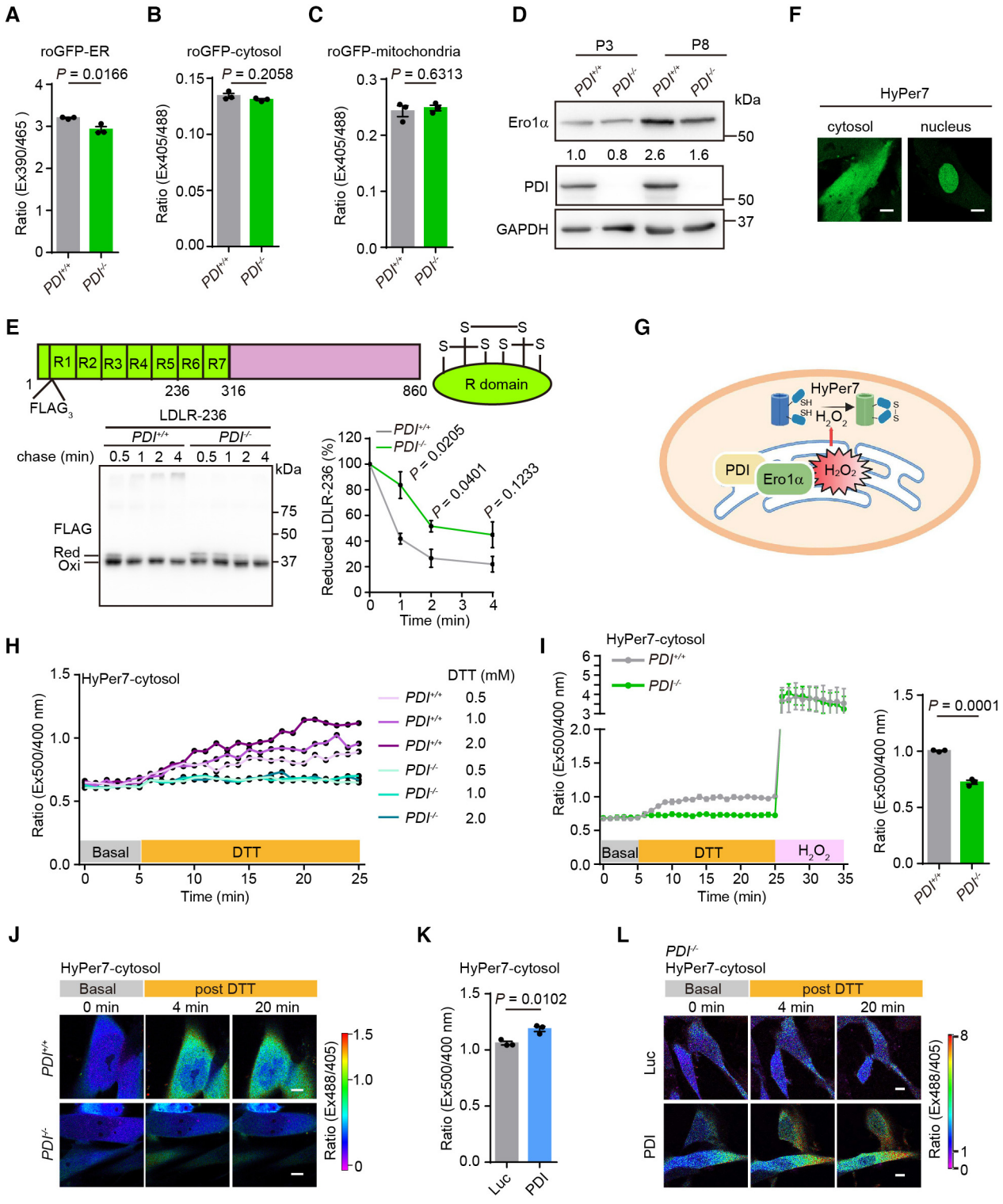

Figure EV3.

Figure EV3. ER-to-cytosol release of H_2O_2 is minimized by PDI deletion.

A–C Glutathione redox states in the ER (A), cytosol (B) and mitochondria (C) of $PDI^{+/+}$ and $PDI^{-/-}$ hMSCs were determined by the fluorescence ratio of roGFP-ER, roGFP-cytosol or roGFP-mitochondria, respectively. $n = 3$ biological repeats.

D Western blotting analysis of Ero1α and PDI expression in $PDI^{+/+}$ and $PDI^{-/-}$ hMSCs at early-passage (P3) and late-passage (P8). GAPDH was used as the loading control.

E Upper, domain organization of LDLR. LDLR contains N-terminally located seven cysteine-rich domains (R1-R7). Lower, oxidative folding of a truncated form of LDLR including domains R1-R5 (LDLR-236). $PDI^{+/+}$ and $PDI^{-/-}$ hMSCs were transfected with LDLR-236 for 48 h, then were pulsed with 5 mM DTT and chased at indicated time after DTT removal. The lysates were analyzed using non-reducing SDS-10% PAGE and α-FLAG western blotting. The mobilities of reduced LDLR-236 monomers (Red), oxidized monomers (Oxi) are indicated. The fraction of reduced LDLR-236 was quantified by densitometry. $n = 3$ independent experiments.

F Confirmation of HyPer7 localization to the cytosol and nucleus. Scale bar, 10 μm.

G Schematic diagram showing the detection of the cytosol H_2O_2 by HyPer7-cytosol upon activation of the Ero1α-PDI oxidative protein folding system in the ER.

H Response of HyPer7-cytosol probes in $PDI^{+/+}$ and $PDI^{-/-}$ hMSCs. The fluorescence intensity ratio of HyPer7-cytosol at 520 nm with excitation at 500/400 nm was firstly monitored at resting state for 5 min, followed by addition of different concentrations of DTT (yellow bar) for another 20 min.

I Left, response of HyPer7-cytosol probes in $PDI^{+/+}$ and $PDI^{-/-}$ hMSCs upon addition of 2 mM DTT for 20 min, followed by addition of 100 μM H_2O_2. Right, statistical analysis of the fluorescence intensity ratio at 500/400 nm excitation of HyPer7-cytosol probe at 20 min post DTT addition. $n = 3$ independent experiments.

J Confocal imaging of $PDI^{+/+}$ and $PDI^{-/-}$ hMSCs expressing Hyper7-cytosol at steady state and upon addition of 2 mM DTT. The fluorescence intensity ratio at 488/405 nm obtained from individual cells was calculated at indicated times with a representative false color image. Scale bar, 10 μm.

K H_2O_2 levels in $PDI^{-/-}$ hMSCs transduced with lentiviruses expressing Luc or PDI were determined by the fluorescence ratio of HyPer7-cytosol at 500/400 nm excitation after the addition of 2 mM DTT for 20 min. $n = 3$ independent experiments.

L Confocal imaging of $PDI^{-/-}$ hMSCs transduced with lentiviruses expressing Luc or PDI and Hyper7-cytosol at steady state and upon addition of 2 mM DTT. The fluorescence intensity ratio at 488/405 nm obtained from individual cells was calculated at indicated times with a representative false color image. Scale bar, 10 μm.

Data information: In (A–C, E, I, K), data are presented as mean ± SEM, two-tailed Student's *t*-test.

Figure EV4. Deficiency of PDI alleviates cell senescence through downregulation of SERPINE1 expression.

A Heatmap showing the Euclidian distance of transcriptome between replicates of $PDI^{+/+}$ and $PDI^{-/-}$ hMSCs at EP and LP.

B, C Volcano plots showing the DEGs between the $PDI^{-/-}$ and $PDI^{+/+}$ hMSCs at EP (B) or LP (C).

D Heatmap showing the Euclidian distance of proteome between replicates of $PDI^{+/+}$ and $PDI^{-/-}$ hMSCs at LP.

E PCA of $PDI^{+/+}$ and $PDI^{-/-}$ hMSCs proteome at LP.

F, G Representative GO terms and pathways enrichment analysis based on upregulated (F) or downregulated (G) DEGs between $PDI^{-/-}$ and $PDI^{+/+}$ hMSCs at LP.

H, I Representative GO terms and pathways enrichment analysis based on upregulated (H) or downregulated (I) DEPs between $PDI^{-/-}$ and $PDI^{+/+}$ hMSCs at LP.

J Venn diagrams showing downregulated DEGs ($PDI^{+/+}$, LP vs $PDI^{+/+}$ EP), upregulated DEGs ($PDI^{-/-}$ LP, vs $PDI^{+/+}$) and upregulated DEPs ($PDI^{-/-}$, LP vs $PDI^{+/+}$, LP).

K Venn diagrams showing upregulated DEGs ($PDI^{+/+}$, LP vs $PDI^{+/+}$ EP), downregulated DEGs ($PDI^{-/-}$ LP, vs. $PDI^{+/+}$) and downregulated DEPs ($PDI^{-/-}$, LP vs. $PDI^{+/+}$, LP).

L, M Representative GO terms and pathways enrichment analysis based on upregulated (L) or downregulated (M) DEGs and DEPs in the LP hMSCs ($PDI^{+/+}$, LP vs. $PDI^{+/+}$, EP) that were restored after PDI deletion at both the proteomic and transcriptional levels ($PDI^{-/-}$, LP vs. $PDI^{+/+}$, LP).

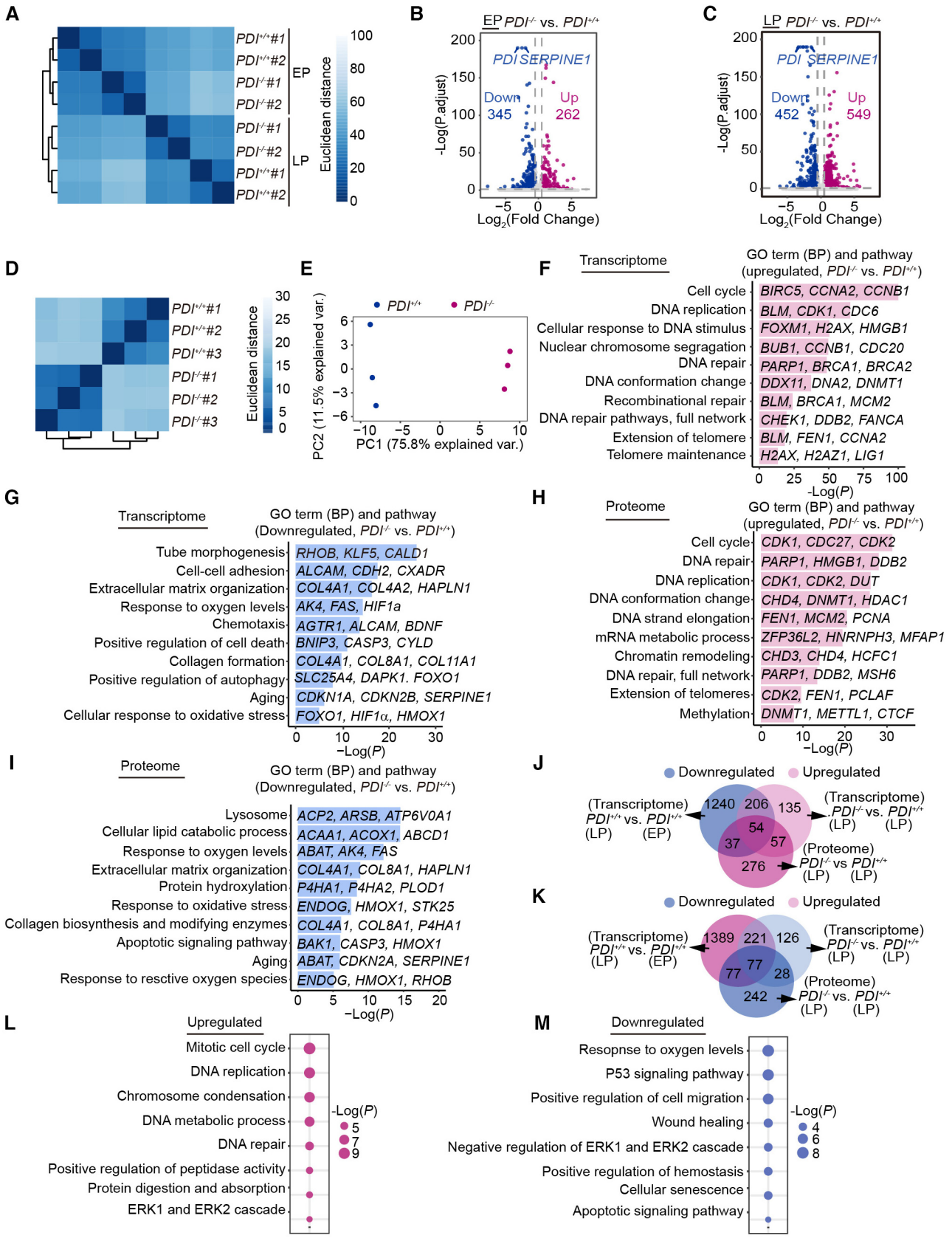

Figure EV4.

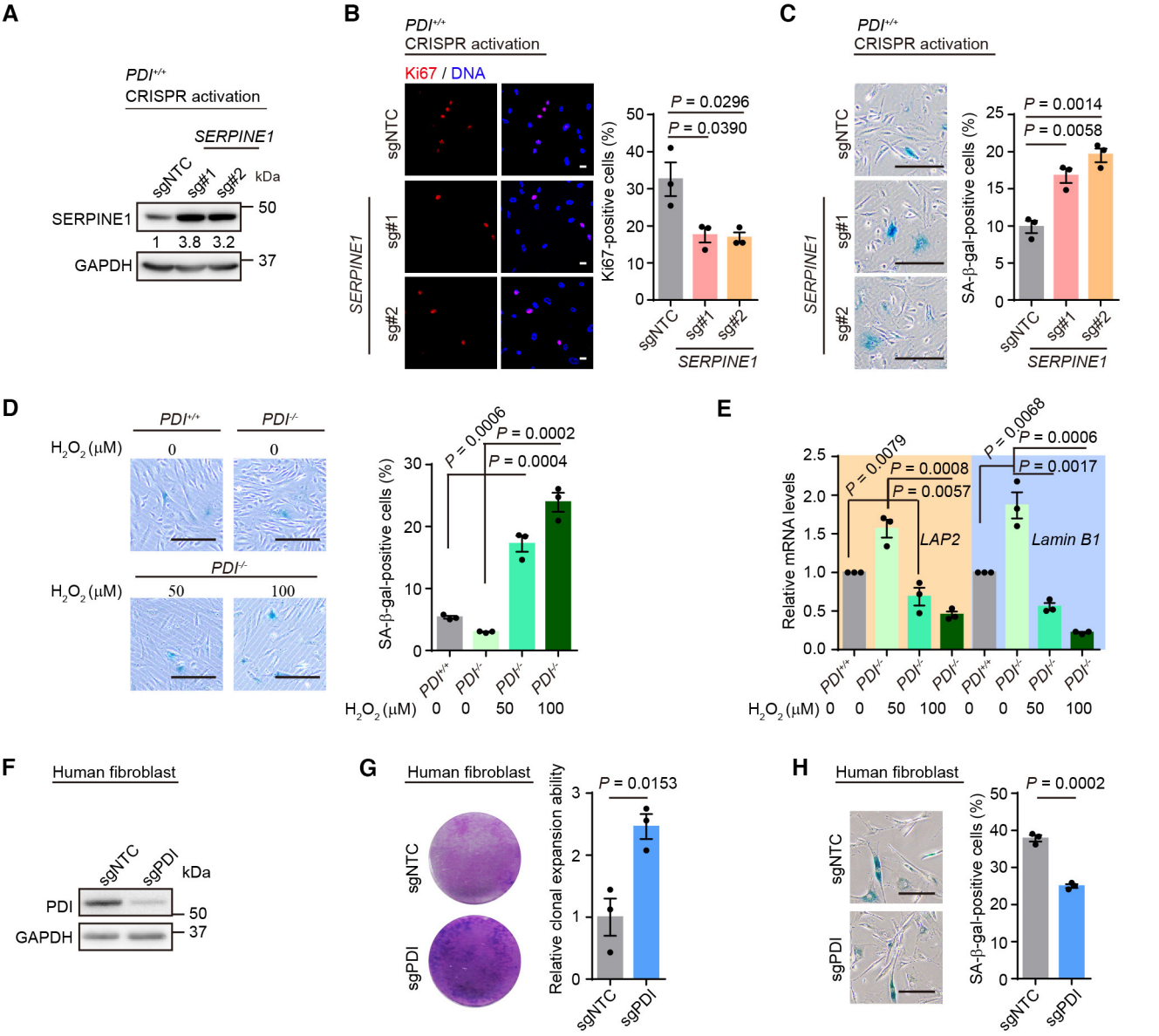

Figure EV5. Upregulation of SERPINE1 induces cell senescence.

A Western blotting of SERPINE1 protein in $PDI^{+/+}$ hMSCs transduced with two *SERPINE1*-targeting activation sgRNAs or sgNTC. GAPDH was used as the loading control.

B Left, Ki67 staining in $PDI^{+/+}$ hMSCs transduced with sgNTC or *SERPINE1*-targeting activation sgRNAs. Scale bar, 20 μm. Right, statistical analysis of Ki67-positive cells. $n = 3$ biological repeats.

C Left, SA-β-gal staining in $PDI^{+/+}$ hMSCs transduced with sgNTC or *SERPINE1*-targeting activation sgRNAs. Scale bar, 200 μm. Right, statistical analysis of SA-β-gal-positive cells. $n = 3$ biological repeats.

D Left, SA-β-gal staining of $PDI^{+/+}$ and $PDI^{-/-}$ hMSCs treated with the indicated concentration H_2O_2 for 4 days. Scale bar, 200 μm. Right, statistical analysis of SA-β-gal-positive cells. $n = 3$ biological repeats.

E qPCR analysis of aging-related genes expression in $PDI^{+/+}$ and $PDI^{-/-}$ hMSCs treated with the indicated concentration H_2O_2 for 4 days. Data are shown as mean ± SEM, $n = 3$ independent experiments.

F Western blotting of PDI expression in human fibroblast transduced with sgNTC or *PDI*-targeting sgRNA. GAPDH was used as the loading control.

G Single clonal formation assay in human fibroblasts transduced with sgNTC or *PDI*-targeting sgRNA. $n = 3$ biological repeats.

H SA-β-gal staining in human fibroblasts transduced with sgNTC or *PDI*-targeting sgRNA. Scale bar, 200 μm. $n = 3$ biological repeat.

Data information: In (B–E, G, H), data are presented as mean ± SEM, two-tailed Student's *t*-test.